Gravitational waves of quasicircular, inspiraling black hole binaries in an ultralight vector-dark-matter environment

Tomás Ferreira Chase,[1,2,*] Diana López Nacir,[1,2,†] and Nicolás Yunes[3,‡]

[1]*Universidad de Buenos Aires, Facultad de Ciencias Exactas y Naturales, Departamento de Física, Buenos Aires, Argentina*

[2]*CONICET—Universidad de Buenos Aires, Instituto de Física de Buenos Aires (IFIBA), Buenos Aires, Argentina*

[3]*Illinois Center for Advanced Studies of the Universe, Department of Physics, University of Illinois at Urbana-Champaign, Urbana, Illinois 61801, USA*

(Received 27 May 2025; accepted 18 September 2025; published 7 November 2025)

The gravitational waves emitted by massive black hole binaries can be affected by a variety of environmental effects, which, if detected, could inform astrophysics and cosmology. We here study how gravitational waves emitted by black holes in quasicircular orbits are affected by the presence of an ultralight, vector field, dark-matter environment that is minimally coupled to the binary. This dark-matter environment induces oscillatory gravitational potentials that perturb the orbit of the binary, leaving an imprint in the binary's binding energy, and thus on the gravitational waves emitted. We here compute the effect of this environment on the gravitational wave phase using the stationary-phase approximation within the post-Newtonian formalism. We then perform a Fisher analysis to estimate the detectability of this environmental effect with a four-year Laser Interferometric Space Antenna (LISA) observation, focusing on vector fields with ultralight masses in the $(10^{-19}, 10^{-16})$ eV range. We conclude that the observation of such gravitational waves with spaceborne interferometers, like LISA, could yield a measurement or constraint on local, vector dark-matter environments, provided the dark-matter density is larger than roughly $10^{14} M_{\odot}/\mathrm{pc}^3$.

DOI: 10.1103/rg4j-8wr9

I. INTRODUCTION

Although there is strong evidence that dark-matter represents approximately 25% of the energy content of the Universe today, its nature still remains unknown. Many dark-matter models (be it wavelike or particlelike) have been considered, with a wide range of masses and interactions. The lightest class of candidates is usually referred to as *ultralight dark-matter* field models, where the mass of the field that describes the dark-matter ranges from $(10^{-28}, 1)$ eV. These candidates have gained attention in recent years due to their agreement with the fiducial ΛCDM model at large scales and their different predictions at small scales [1–4].

One distinctive feature of ultralight dark-matter candidates is that they induce oscillatory gravitational potentials. The frequency of the oscillations is determined essentially by the mass of the ultralight dark-matter particles. In cosmological contexts, the dark-matter field oscillations usually average out, but this need not be the case around astrophysical systems. In fact, previous work has shown that an oscillatory ultralight, dark-matter environment induces oscillatory behavior in the spacetime metric of astrophysical systems, for example, impacting the orbital dynamics and evolution of binary pulsars [5–7]. Could such an ultralight, dark-matter environment also affect the gravitational waves emitted by compact binaries?.

General relativity predicts that gravitational waves are excited by any system with a nontrivial, time-varying multipole-moment structure, such as due to the orbital acceleration of a binary system. When in isolation, the orbital dynamics and evolution of inspiraling compact binaries can be determined from perturbative solutions to the Einstein equations. In practice, when the compact binary is sufficiently well separated, one employs a post-Minkowskian expansion (in weak fields) or a post-Newtonian expansion (in both weak fields and small velocities) to calculate the gravitational waves in the inspiral phase of coalescence from first principles [8]. When not in isolation, for example, due to the presence of an accretion disk [9–11] or a dark-matter environment [12,13], the orbital dynamics and evolution of inspiraling compact binaries is in general modified, leaving an environmental imprint on the gravitational waves generated.

*Contact author: tferreirachase@df.uba.ar
†Contact author: dnacir@df.uba.ar
‡Contact author: nyunes@illinois.edu

The question is then not whether an ultralight, dark-matter environmental imprint is present in gravitational waves, but rather whether this imprint is *detectable*.

One of the most studied phenomenons connecting dark-matter fields and black holes is the *superradiant instability*, which leads to the formation of a bosonic condensate around spinning black holes [14–17]. Such studies lead to the following exclusion windows for the mass of the vector field at a 68% confidence limit [18]: 6.2×10^{-15} eV $\leq m \leq 3.9 \times 10^{-11}$ eV, $2.8 \times 10^{-22}\,\text{eV} \leq m \leq 1.9 \times 10^{-16}\,\text{eV}$, which incorporate observations of the event GW190521 and the shadow of M87*. In this paper, we focus on a different phenomenon than the one studied in previous work. In our setup, for the sake of simplicity, we consider black holes with negligible spins so that the formation of a condensate via superradiance can be neglected.

Recent efforts have also been made to search for the direct imprint of ultralight dark-matter in gravitational waves. For example, in [19,20], the dephasing of gravitational waves produced by dark-matter fields was considered. In these works, the dephasing is produced in the propagation of the gravitational wave signal from the source to the detector, caused by the gravitational potentials generated by the ultralight dark-matter fields. In this work, however, we focus on how these gravitational potentials create a dephasing in the *generation* of the gravitational wave signal, by changing the worldline of the binary system components, rather than by correcting the way the gravitational waves propagate.

When the binary systems emitting gravitational waves are immersed in a virialized ultralight, dark-matter halo, the dark-matter that forms the halo (be it scalar or vector particles) can be described as a collection of waves with random phases [21–24]. These waves induce oscillations in the spacetime metric, which then perturb the orbital motion of the binary. In particular, the ultralight dark-matter oscillations induce a correction to the acceleration of the binary components, which then affects the orbital energy and angular momentum, introducing dark-matter corrections to Kepler's third law. The ultralight dark-matter environment, therefore, perturbs the orbital motion of the binary, which then leaves an imprint on the time-varying multipole-moment structure of the spacetime, and thus on the gravitational waves emitted. Given this, one expects the strength of the dark-matter imprint on the emitted gravitational waves to be proportional to the dark-matter density and sensitive to the dark-matter mass, which sets the dark-matter oscillation scale, especially close to resonances between this oscillation scale and the orbital timescale.

In this paper, we explore the possibility of detecting such ultralight dark-matter effects (for a vector dark-matter model) through the gravitational waves emitted by massive black hole binaries immersed in such a dark-matter environment and detected (in the future) with the spaceborne Laser Interferometric Space Antenna (LISA). Figure 1 presents

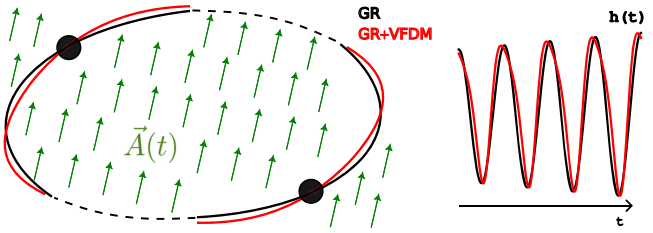

FIG. 1. Cartoon illustration of the dark-matter environment effect on the orbit (left) and on the gravitational waves (right) due to an ultralight vector field (green arrows).

a cartoon illustration of the problem we tackle. We first use post-Newtonian theory to calculate the dark-matter corrections to the orbital binding energy and Kepler's third law. For scalar field, ultralight, dark-matter models, this effect vanishes for circular orbits, as a consequence of the symmetry of the configuration. For vector field, ultralight, dark-matter models, however, this symmetry is broken thanks to the anisotropic nature of the vector field. We thus focus on quasicircular orbits and calculate the vector ultralight dark-matter corrections to the Fourier domain gravitational wave phase, using the stationary-phase approximation.

As we show in the paper, the strength of the ultralight dark-matter effect on the gravitational waveform is proportional to the energy density $\rho_{\rm DM}$ of the dark-matter field in the surroundings of the black hole binary. Several works [25,26] have estimated the dark-matter density in our Solar System to be $\rho_{\rm DM} \sim 0.3\ \text{GeV/cm}^3 \sim 0.01 M_\odot/\text{pc}^3$. However, the dark-matter density distribution in galaxies is still a matter of debate. In particular, the dark-matter distribution surrounding black holes remains uncertain and varies depending on the dark-matter model. For example, various works [27–32] suggest that scalar and vector field models in the particle regime ($\lambda_c \sim m^{-1} \ll r_s$, with r_s being the black hole Schwarzschild radius) *spike* near black holes, where the density may be several orders of magnitude bigger than the one estimated for our Solar System. In our work, we consider fields and black holes that are in the wave regime ($\lambda_c \gg r_s$), where the existence of a local density enhancement is unclear. We find that the vector ultralight dark-matter corrections are indeed proportional to the dark-matter density, and inversely proportional to a certain power of the ultralight dark-matter mass and the total mass of the binary. Moreover, we find that when the gravitational wave frequency exceeds a certain threshold, given by a stationary point condition that depends on the vector field mass, the ultralight dark-matter corrections are strongly suppressed. On the other hand, when the gravitational wave frequency is below this threshold, the vector ultralight dark-matter effect on the gravitational wave phase for quasicircular orbits is partially degenerate with the time and phase of coalescence of the binary, rendering this effect hard to measure. This leads to a Heaviside-type modification to the Fourier transform of the gravitational wave

phase, and it is this sudden turn-on/turn-off nature of the modification that yields the dark-matter effect potentially measurable.

Our work suggests that chirping, massive binaries that sample a range of frequencies in the LISA band (and thus, that cross the stationary point condition activating the Heaviside dark-matter modifications) are necessary to observe this type of dark-matter effect. Through a Fisher analysis, we estimate that LISA would be able to constrain the ultralight dark-matter mass range $(10^{-19}, 10^{-16})$ eV for gravitational waves emitted by massive $[(10^2, 10^6)M_\odot]$ black hole binaries of comparable mass, provided the ultralight dark-matter density is above $(10^{14}, 10^{15})M_\odot$ pc^{-3}. Our work, therefore, suggests that future LISA observations of the gravitational waves emitted in the quasicircular inspiral of massive black holes may detect or yield interesting constraints on the density of vector-type ultralight dark-matter.

The remainder of this paper presents the derivation of the results summarized above, and it is organized as follows. In Sec. II, we present the vector field dark-matter model, while in Sec. III, we solve for the evolution of the vector field and its backreaction onto the perturbations of the spacetime metric. In Sec. IV, we show how the presence of a vector field dark-matter component changes the evolution of the orbital parameters of a binary system. In Sec. V, we calculate the vector ultralight dark-matter modifications to the gravitational waves emitted by quasicircular inspiraling binaries, as a consequence of the vector field environment. In Sec. VI, we present a Fisher analysis and compute the parameter space of the vector field dark-matter model that would be detectable given a LISA observation of massive black hole binaries. Henceforth, we switch between geometric units (where $G = 1 = c$) and natural units (where $\hbar = 1 = c$) and, therefore, we sometimes quote masses in units of length and sometimes in units of energy. The conversion is, of course, simple with, for example, $\tilde{m} = cm/\hbar$ in units of length when m is in units of electron-volts.

II. ULTRALIGHT DARK-MATTER VECTOR FIELD AROUND A COMPACT BINARY

In this section, we present the vector field dark-matter model that we study in this paper, following mostly [7], for completeness and to establish notation. Let us then describe the dark-matter through an ultralight vector field minimally coupled to gravity, whose action is

$$\mathcal{S} = \int dx^4\sqrt{-g}\left[R - \frac{1}{4}F^{\mu\nu}F_{\mu\nu} - \frac{m_A^2}{2}A^\mu A_\mu + \mathcal{L}_M\right], \tag{1}$$

where R is the Ricci scalar, g is the determinant of the metric, $\mathcal{L}_M$ is the Lagrangian of the ordinary matter sector, and $F_{\mu\nu} = \nabla_\mu A_\nu - \nabla_\nu A_\mu$ is the field strength tensor of the massive vector field A^μ, with mass m_A. Since we assume that the vector field makes up all the dark-matter in the Universe, we have a lower bound on the boson mass of $m_A > H_{\rm eq} \sim 10^{-28}$ eV, where $H_{\rm eq}$ is the Hubble parameter at the moment of equality between the energy density of the radiation and matter content of the Universe.

The equations of motion of the vector field can be derived by varying the action with respect to the field, thus obtaining

$$\nabla_\mu F^{\mu\nu} + m_A^2 A^\nu = 0, \tag{2}$$

since there is no direct (nonminimal) coupling of the vector field with the gravitational sector. Similarly, the equations of motion for the metric can be derived by varying the action with respect to the metric, obtaining

$$G^\mu{}_\nu = 8\pi G T^\mu_{A\nu} + 8\pi G T^\mu_{M\nu}, \tag{3}$$

where $G^\mu{}_\nu$ is the Einstein tensor, and $T^\mu_{A\nu}$ and $T^\mu_{M\nu}$ are the stress-energy tensors of the vector field and the ordinary matter sector, respectively. We calculate the stress energy of the vector field as usual, $T^A_{\mu\nu} = -(2/\sqrt{g})(\delta\mathcal{S}_A/\delta g^{\mu\nu})$, where $\mathcal{S}_A$ is the action of the vector field, to find

$$T^\mu_{A\nu} = F^{\mu\gamma}F_{\nu\gamma} - \frac{\delta^\mu{}_\nu}{4}F^{\mu\nu}F_{\mu\nu} - m_A^2\left(A^\mu A_\nu + \frac{\delta^\mu{}_\nu}{2}A^\mu A_\mu\right), \tag{4}$$

which is symmetric, as expected.

In this paper, we study the effect of vector dark-matter on an inspiraling binary system that emits gravitational waves in the millihertz band. Therefore, the stress-energy tensor for ordinary matter represents a compact binary, composed of intermediate-mass and supermassive black holes. For simplicity, we assume the binary is in a quasicircular inspiral orbit and that the black holes are not spinning, leaving extensions of our work to eccentric orbits and spinning black holes for the future.

We consider that the vector dark-matter field around a compact binary can be described as a classical wave characterized by an amplitude, phase, and direction[1] that can be considered to be constant within a certain characteristic volume during a characteristic time interval. We will refer to such spacetime volume as a coherent patch. The vector field in different coherent patches can have very different amplitudes, phases, and directions. Our model is based on numerical simulations. In Refs. [21,24], the authors study the merger of idealized halos, usually called *solitons*, to characterize small-scale structure formation with vector field dark-matter. As was shown in such spin-1 halo-scale simulations, the system evolves into an

[1]We assume that the background vector field is linearly polarized. However, this is not a necessary condition for the local vector field in the halo. For example, in [21,33] the authors perform small-scale structure simulations with vector field dark-matter with different polarizations for the background field.

approximately spherical configuration that has a core surrounded by a dark-matter density distribution characterized by interference patterns. The characteristic size of the interference granules is given by the de Broglie wavelength of the particle $\lambda_{\rm dB}$. This is similar to what has been shown for scalar field dark-matter models (see, for instance, Refs. [23,34,35]). Due to the evolution of the interference patterns, at a given point in space the field loses coherence after a time that can be estimated as $t_{\rm coh} \sim \lambda_{\rm dB}/V_0$, where V_0 is the local velocity of the dark-matter field. These characteristic scales ($\lambda_{\rm dB}$ and $t_{\rm coh}$) define the typical spacetime size of the coherent patches.

We focus on binary systems living inside one of these patches, characterized by a constant dark-matter energy density. Then, a given binary system is immersed in a vector field environment that is homogeneous over the size of the binary and the gravitational wavelength of the waves emitted by the binary. More concretely, if the binary separation is r_{12} and the orbital velocity is v_{12}, then the wavelength of the gravitational waves is $\lambda_{\rm GW} = r_{12}/v_{12}$, and we require that $r_{12} \ll \lambda_{\rm GW} \ll \lambda_{\rm dB}$, with $\lambda_{\rm dB}$ being the local de Broglie wavelength of the boson. For the ultralight masses considered in this work $(10^{-19}, 10^{-16})$ eV and for the binaries that can be probed by spaceborne detectors, the de Broglie wavelength of the boson $\lambda_{\rm dB}$ is much larger than the orbital separation of such compact binary systems, $\lambda_{\rm dB} \gg r_{12}$. Indeed, the de Broglie wavelength of the boson is

$$\lambda_{\rm dB} \sim 1.3 \times 10^{12} \left(\frac{10^{-3}}{V_0}\right) \left(\frac{10^{-18}\ \text{eV}}{m_A}\right)\ \text{km}, \tag{5}$$

where V_0 is the velocity dispersion of the halo, which can be estimated from the virial velocity, e.g., $V_0 \sim 10^{-3}$ for the Milky Way. On the other hand, for the systems that can be probed by LISA with a high signal-to-noise ratio, such as supermassive black holes of $M \sim 10^6 M_\odot$, the largest separations correspond[2] to the lowest frequencies LISA is sensitive to, $f \sim 10^{-5}$ Hz. Using Kepler's third law we can calculate the semimajor axis of such systems, giving

$$r_{12} \sim 3.2 \times 10^{8} \left(\frac{M}{10^6 M_\odot}\right)^{\frac{1}{3}} \left(\frac{f}{10^{-5}\ \text{Hz}}\right)^{-\frac{2}{3}}\ \text{km}, \tag{6}$$

and for the corresponding emitted gravitational wave, $\lambda_{\rm GW} \sim 10^{10}$ km. Furthermore, for $m_A < 10^{-16}$ eV, we have

$$t_{\rm coh} \sim 65\ \text{yrs} \left(\frac{10^{-3}}{V_0}\right)^2 \left(\frac{10^{-18}\ \text{eV}}{m_A}\right), \tag{7}$$

so for the field masses considered in this work the patch remains coherent during a typical LISA observation, which ranges from one year to four years. In summary, we find that the de Broglie wavelength is much larger than the orbital separation of the binary, and during the observation, the patch remains coherent. We, therefore, expect the background vector field (and its associated metric perturbation) to be approximately *homogeneous* at scales comparable to the size of the binary system, i.e., $\bar{A}^\mu$ and $h^A_{\mu\nu}$ are approximately independent of spatial coordinates and only depend on time. In the Appendix we give a more detailed discussion of the previous assumption, based on numerical simulations.

We assume that the binary system and the vector field produce small departures from a background vacuum metric, both of which can be treated perturbatively. Thus, we start by splitting the metric and the vector field as

$$g_{\mu\nu} = \bar{g}_{\mu\nu} + h^A_{\mu\nu} + h^M_{\mu\nu}, \tag{8}$$

$$A_\mu = \bar{A}_\mu + \delta A_\mu, \tag{9}$$

where $\bar{g}_{\mu\nu}$ and $\bar{A}_\mu$ are the background metric and vector field, respectively, while the metric perturbations $h^A_{\mu\nu}$ and $h^M_{\mu\nu}$ are produced by the vector field and the binary system, respectively. The quantity δA_μ is a small perturbation that we will neglect henceforth, but that in principle includes inhomogeneities and the backreaction of the binary on the vector field. We here ignore the cosmological expansion of the Universe and assume the background metric is the flat Minkowski spacetime,[3] $\bar{g}_{\mu\nu} = \eta_{\mu\nu}$. Thus, when we ignore the presence of the vector field, the metric perturbation $h^M_{\mu\nu}$ is nothing but the post-Newtonian solution for an inspiraling binary, as reviewed, for example, in [8].

With this setup, we wish to study the effect of the vector field metric perturbation $h^A_{\mu\nu}$ on the metric perturbation induced by the binary system $h^M_{\mu\nu}$, and we do so by expanding the field equations (Einstein plus vector field) in both perturbations. Given the above, the setup of the problem lends itself perfectly to the technique of separation of scales when solving the perturbed field equations. We now proceed to solve the field equations with the assumptions described above. First, we work at the largest scales and solve for (i) the vector field and (ii) the metric perturbation induced by the vector, in both cases ignoring the ordinary matter sector. That is, we first solve

$$\nabla_\eta F^{\mu\nu}[\bar{A}_\alpha] + m_A^2 \bar{A}^\nu = 0, \tag{10}$$

[2]In principle, LISA can detect binaries with lower masses at much larger separations (which would merge in the band of ground-based detectors), but at much lower signal-to-noise ratios, since the latter scales with the total mass.

[3]The typical timescales of a gravitational wave detector (∼years) are much smaller than the Hubble time in the matter era, and the main correction due to cosmic expansion is a redshift in the wavelength of the propagating gravitational wave [36].

where ∇_η is the covariant derivative with respect to the Minkowski metric and $F^{\mu\nu}[\bar{A}_\alpha]$ is the field strength tensor associated with the background vector field. This is an equation of $\mathcal{O}(\bar{A}^\mu)$, which gives us a background solution for the vector field $\bar{A}^\mu$. Given this solution, we then solve

$$G_{\mu\nu}[h^A_{\alpha\beta}] = 8\pi T^A_{\mu\nu}[\bar{A}_\alpha], \tag{11}$$

where $G_{\mu\nu}[h^A_{\alpha\beta}]$ is the part of the linearized Einstein tensor that depends on $h^A_{\alpha\beta}$, while $T^A_{\mu\nu}[\bar{A}_\alpha]$ is the part of the linearized stress-energy tensor that depends on $\bar{A}^\mu$. This is an equation of $\mathcal{O}(\bar{A}^\mu\bar{A}_\mu)$, which gives us a solution for the metric perturbation $h^A_{\mu\nu}$ induced by the vector field $\bar{A}_\alpha$.

With this in hand, we then focus on the metric perturbation induced by the ordinary matter sector. In the absence of the vector field, the solution for $h^M_{\mu\nu}$ can be obtained through standard post-Newtonian methods [8], as discussed earlier. We then need to understand the backreaction of the vector field $\bar{A}^\mu$ on $h^M_{\mu\nu}$. The dominant correction to this metric perturbation is that induced by the correction to the trajectories of the binary system, which, as we will see, is effectively a conservative force induced by $\bar{A}^\mu$ that modifies the binary's binding energy. By the balance law, this modification then alters the evolution of the orbital frequency, and thus the gravitational wave phase. This is the main and largest effect we consider in this paper, and thus we leave the full backreaction of $h^A_{\mu\nu}$ on $h^M_{\mu\nu}$ and vice versa to future work (see Appendix for a discussion).

III. EVOLUTION OF THE BACKGROUND ULTRALIGHT DARK-MATTER VECTOR FIELD AND ITS METRIC PERTURBATION

Following the considerations in the previous section, we model the vector dark-matter field in one coherent patch as a homogeneous vector field $\bar{A}^\mu$, and calculate its associated metric perturbation. The dynamics of the background vector field is given by Eq. (10). From this equation, we can extract a constraint equation for the temporal component and three equations of motion for the spatial components. As we discussed earlier, we can assume that the background vector field is spatially homogeneous, $\bar{A}^\mu = \bar{A}^\mu(t)$. Under this assumption, the temporal component of the background vector field exactly vanishes, $\bar{A}^0 = \bar{A}_0 = 0$, while the spatial components satisfy the equations of motion

$$\ddot{\bar{A}}_i + m_A^2\bar{A}_i = 0, \tag{12}$$

where the overhead dots stand for time derivatives. This equation of motion can be solved as a harmonic oscillator for each component,

$$\bar{A}^i(t) \sim \tilde{A}\cos(m_A t + \gamma)\hat{A}^i, \tag{13}$$

where $\tilde{A}$ is a constant amplitude, γ is a constant phase, both determined by the initial conditions, and $\hat{A}^i$ is a unit vector pointing in the direction of the vector field.

With this background vector field, we can now search for solutions to the metric perturbation it generates, which is given by Eq. (11). In the binary's source frame, the metric perturbations can be decomposed in the Newtonian gauge as

$$h^A_{00} = 2\phi, \qquad h^A_{0i} = B_i, \qquad h^A_{ij} = -2\psi\delta_{ij} + 2E_{ij}, \tag{14}$$

where $(\phi, \psi, B_i, E_{ij})$ are metric perturbation functions of time only, which satisfy $B^i{}_{,i} = 0$ and $E^i{}_{j,i} = E^i{}_i = 0$. At linear order in the metric perturbations, the spatial components of Eq. (11) then become

$$2\ddot{\psi}\delta^i{}_j + \ddot{E}^i{}_j - \partial^{(i}\dot{B}_{j)} = 8\pi G T_A{}^i{}_j[\bar{A}^\mu], \tag{15}$$

where the energy-momentum tensor on the right-hand side is the part of the linearized stress-energy tensor that depends on the background vector field.

By considering a homogeneous field in flat spacetime, we can further simplify the stress-energy tensor given in Eq. (4). First, we note that $-\frac{1}{2}F^{\mu\nu}F_{\mu\nu} + m_A^2A^\mu A_\mu = -\dot{A}^2 + m_A^2A^2$ and $F^{\mu\gamma}F_{\nu\gamma} = \dot{A}^2$, where the square means the spatial norm in flat spacetime. Then, the components of the energy-momentum tensor for the homogeneous field are

$$T_A{}^0{}_0 = -\frac{m_A^2\tilde{A}^2}{2} \equiv -\rho_A, \tag{16a}$$

$$T_A{}^0{}_j = 0, \tag{16b}$$

$$T_A{}^i{}_j = \rho_A\cos(2m_A t + \gamma)\hat{X}^i{}_j \equiv P_A\delta^i{}_j + \Sigma^i_{Aj}, \tag{16c}$$

where $\hat{X}^i{}_j = \delta^i{}_j - 2\hat{A}^i\hat{A}_j$. We have identified the time-time component of the stress-energy tensor as the energy density ρ_A of the vector field in the local patch, which on the timescales considered here is approximately constant. The space-space components can be split into a trace part, given by the pressure of the field P_A, and a traceless part Σ^i_{Aj}, which can be identified as the shear of the field. The presence of the shear in the energy-momentum tensor is a main difference with respect to ultralight scalar field models. In particular, the shear is responsible for inducing a nonvanishing effect on circular orbits, in contrast with scalar models, where the effect vanishes due to the symmetry of the configuration.

Now we return to the Einstein equations. As will become clear in the next section, to study the impact of the vector field dark-matter on the trajectories of the binary system, and thus the gravitational wave metric perturbation, we need Eq. (15). With the above stress-energy tensor, this equation simplifies to

$$-2\ddot{\psi}\delta^i{}_j - \partial^{(i}\dot{B}_{j)} - \frac{1}{2}\ddot{E}^i{}_j = 8\pi G\rho_A \cos(2m_A t+\gamma)\hat{X}^i{}_j. \quad (17)$$

As we will show in Sec. V, the energy density of the field controls the magnitude of the correction to the trajectories of the binary system, and thus the gravitational wave phase evolution.

IV. IMPACT OF ULTRALIGHT DARK-MATTER VECTOR FIELD ON THE ORBITAL MOTION OF A COMPACT BINARY

In this section we consider the impact of the oscillating gravitational potentials governed by Eq. (17) on the binary orbit. We start by considering two masses bound gravitationally in a circular orbit of radius $R(t)$, neglecting the gravitational wave backreaction. We place the origin of coordinates at the center of mass of the system, and transform the problem into an effective one-body one, where a point particle (or test mass) with mass equal to the reduced mass μ of the binary is in orbit around a gravitating object with mass equal to the total mass of the binary M. The position of the reduced mass particle is denoted by $r^i(t) = r^i_1 - r^i_2$, where r^i_1 and r^i_2 are the positions of the two masses in the real problem. The binary system is immersed in a vector field dark-matter background, which is approximately homogeneous at scales of $\mathcal{O}(|r^i|)$, but time dependent. The field is pointing in an arbitrary direction (parametrized in terms of two angles, α and φ) with respect to the orbital plane, which we assume to be constant in time. For an illustration of the configuration, see Fig. 2.

The oscillating potentials induced by the vector field dark-matter environment cause small deviations in the system's orbit. These deviations can be captured in general relativity through the vector field corrections to the *geodesic deviation equation*. In other words, in the effective one-body problem, the test particle follows a geodesic (neglecting gravitational wave backreaction) in the geometry of the larger body, but this geodesic is perturbed by vector field effects. The perturbations to the geodesic motion can be captured through the geodesic deviation equation. In the weak field approximation and using Fermi normal coordinates, the geodesic deviation equation for the reduced mass reads

$$\frac{d^2 r^i}{dt^2} = (R^i{}_{0j0}[h^A_{\mu\nu}] + R^i{}_{0j0}[h^M_{\mu\nu}])r^j \quad (18)$$

to first order in metric perturbations, where $R^i{}_{0j0}[h^A_{\mu\nu}]$ and $R^i{}_{0j0}[h^M_{\mu\nu}]$ are the components of the linearized Riemann tensor associated with the metric perturbations generated by the vector field and the binary system, respectively.

The contribution from the binary system to the linearized Riemann tensor in Eq. (18), $R^i{}_{0j0}[h^M_{\mu\nu}]$, yields the post-Newtonian equations of motion in the center-of-mass frame. In particular, when the metric perturbation $h^M_{\mu\nu}$ is taken to leading post-Newtonian order, one obtains the usual Newtonian law of gravity, i.e., $R^i{}_{0j0}[h^M_{\mu\nu}]r^j = -(GM/r^2)r^i$ (see, for instance, Sec. 17.4 in [37]). The contribution from the vector field can then be interpreted as a perturbation to the post-Newtonian equations of motion. The components of $R^i{}_{0j0}[h^A_{\mu\nu}]$ can be written in terms of the vector field fluid variables using Eq. (17), as

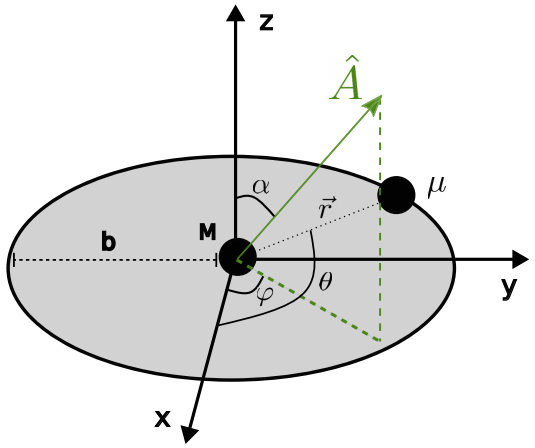

FIG. 2. Diagram of the effective one-body problem. The origin of the coordinates is placed at the center of mass of the binary, and the position of the reduced mass is described by the vector $\vec{r} = b[\cos(\theta)\hat{x} + \sin(\theta)\hat{y}]$. The green arrow points in the direction of the vector field, which is defined with the angles φ and α.

$$R^i{}_{0j0}[h^A_{\mu\nu}] = -\delta^i{}_j\ddot{\psi} - \frac{1}{2}\ddot{E}^i{}_j + \frac{1}{2}\partial^{(i}\dot{B}_{j)}, \quad (19)$$

$$= -4\pi\rho_A \cos(2m_A t+\gamma)\hat{X}^i{}_j. \quad (20)$$

Inserting the previous expression in Eq. (18), we obtain the modified Newtonian equation for the binary system in the vector field environment,

$$\vec{a} + \frac{GM}{r^2}\hat{r} = -4\pi\rho_A r\,\cos(2m_A t+\gamma)[\hat{r} - 2(\hat{r}\cdot\hat{A})\hat{A}], \quad (21)$$

where $\vec{a}$ is the relative acceleration between the bodies and we have here kept the post-Newtonian equations of motion to leading order only (and moved the Newtonian gravitational acceleration to the left-hand side).

The effect of the vector field environment on the orbit can be interpreted as a perturbation to the usual Newtonian law of gravity. We thus identify the right-hand side of Eq. (21) as a perturbative force per mass unit that the vector field exerts over the binary system. The corresponding produced acceleration can then be written as

$$f^i = -4\pi\rho_A \cos(2m_A t+\gamma)r^j\hat{X}^i{}_j, \quad (22)$$

where we recall that $\hat{X}^i{}_j = \delta^i{}_j - 2\hat{A}^i\hat{A}_j$. Moreover, since the unperturbed problem reduces to Newtonian gravity,

we know that Kepler's laws are valid to leading order, so the frequency of the orbit is $\omega^2 \sim M/r^3 + \mathcal{O}(\rho_A)$, and the binding energy of the orbit is the usual Newtonian potential, namely, $E_M \sim -G\mu M/2r + \mathcal{O}(\rho_A)$.

The acceleration in Eq. (22) can be derived from the following time-varying potential:

$$V_A = 2\pi\mu\rho_A \cos(2m_A t + \gamma)[\vec{r}^2 - 4(\vec{r}\cdot\hat{A})^2], \quad (23)$$

where $f_i = -\partial_i V_A$. This potential is invariant under time reversal,[4] and thus the force associated with it is conservative. The binding energy of the system is then modified to be $E = E_M + V_A$. The perturbation V_A, despite being time varying, does not change the binding energy, on average over timescales of order m_A^{-1} or $1/\omega$, with ω being the angular frequency of the orbit. In this paper, we consider binary systems in the LISA band, over an observation period of order one year, so the binding energy is not modified on average. However, as we show in Sec. V, this perturbation does impact the gravitational waveform.

The perturbation in the binding energy V_A induces a perturbation in the evolution of the semimajor axis of the orbit, given by the oscillating potentials generated by the vector field. Let us now calculate this variation with the *method of osculating orbits*, which is ideally suited to perturbations of Keplerian orbits. This method gives the equations of motion for the parameters that are otherwise conserved in the usual Kepler problem. To calculate the variation in the semimajor axis b, it is convenient to decompose the acceleration in a polar basis, given by $\{\hat{r}, \hat{\theta}, \hat{z}\}$, as

$$\vec{f} = f_r\hat{r} + f_\theta\hat{\theta} + f_z\hat{z}, \quad (24)$$

where $\hat{z}$ is normal to the orbital plane. In this basis, one can show that the equation of motion for the semimajor axis of a circular orbit is given by[5]

$$\dot{b} = \frac{2}{\omega} f_\theta, \quad (25)$$

where $\omega = 2\pi/P = \sqrt{GM/b^3}$ by Kepler's third law, and P is the orbital period.

The method of osculating orbits also predicts variations in other orbital parameters due to the presence of the vector field environment, such as a variation in the orbital eccentricity, or in the relative inclination angle ι between the orbit plane and the observation plane. However, we here neglect such effects and leave them for future work for the following reasons. The variation in the angle ι can be neglected because it only impacts the gravitational wave amplitude (for nonspinning binaries), which in general is harder to measure in comparison to perturbations in the gravitational wave phase (such as the contribution from $\dot{b}$ we consider here). Moreover, general relativity is very efficient at circularizing orbits through gravitational wave emission, so in the regime where the vector field effect is much smaller than those in general relativity, it is a good approximation to work in the quasicircular limit, and we can neglect any dark-matter excitation of the eccentricity.

The equation of motion for the semimajor axis [Eq. (25)] deserves further discussion. First, we see that, for circular orbits, we have a nonzero perturbation of the orbit, as long as the perturbing forces have tangential components. Scalar field models do not have tangential components due to the symmetry of the field. Fields of higher spin, however, can break this symmetry, thus producing a nonvanishing effect, even for circular orbits. Note also that the perturbing force is conservative, so the temporal evolution of the semimajor axis is also conservative and, in particular, it is not driven by dissipative forces. Gravitational wave backreaction is a dissipative effect that also induces a time variability in the semimajor axis, forcing the binary to inspiral, but this backreaction effect is qualitatively different from the conservative effect of the perturbing vectorial force studied here.

Let us now calculate the components of the force using Eq. (22). To do this, it is convenient to write the vector field in spherical polar coordinates, as $\hat{A} = \sin(\alpha)\cos(\varphi)\hat{x} + \sin(\alpha)\sin(\varphi)\hat{y} + \cos(\alpha)\hat{z}$, where $\hat{x}$-$\hat{y}$ is the orbital plane. The position of the reduced mass on the orbital plane in polar coordinates can then be written as $\vec{r} = b[\cos(\theta)\hat{x} + \sin(\theta)\hat{y}] + z\hat{z}$. For a diagram of the configuration, see Fig. 2. With this in hand, we obtain the tangential component of Eq. (22) at $z = 0$,

$$(f_\theta)_A = 8\pi\rho_A b\, \cos(2m_A t + \gamma)\sin(2\varphi - 2\theta)\sin(\alpha)^2. \quad (26)$$

Observe that the force is proportional to the dark-matter density ρ_A, as expected. Observe also that the force vanishes if the vector is exactly orthogonal to the orbital plane, since then the vector field would not exert any tangential force.

We can now calculate the equation of motion of the semimajor axis by inserting the vector field force [Eq. (26)] in the Keplerian expression for $\dot{b}$, given in Eq. (25). By considering the conservative contribution from the vector field environment, we obtain that the variation in the semimajor axis is

[4]The phase angle γ is set by the initial conditions to the solution of the vector field equation of motion. In particular, γ depends on the initial velocity of the vector field, which flips sign under time reversal. Therefore, to keep the initial conditions invariant under time reversal, then $\gamma \to -\gamma$ when $t \to -t$. With this, under time reversal, $\cos(2m_A t + \gamma) \to \cos(-2m_A t - \gamma) = \cos(2m_A t + \gamma)$.

[5]For a detailed derivation of the osculating equations, see, for instance, Sec. 3.3 of Ref. [38].

$$\left(\frac{\dot{b}}{b}\right)_A = \frac{16\pi G\rho_A}{c^2\omega}\cos(2m_A t+\gamma)\sin(2\varphi-2\omega t)\sin(\alpha)^2. \tag{27}$$

As mentioned earlier, the perturbation to the semimajor axis vanishes when the vector field is normal to the orbital plane, due to the symmetry of the circular orbit. Observe also that the perturbation is greatest when the vector is parallel to the orbital plane.

How large is this perturbation relative to other perturbations we expect the binary system to experience? The main other perturbation is gravitational wave backreaction, which induces a change in the semimajor axis of the form [39]

$$\left(\frac{\dot{b}}{b}\right)_M = -\frac{64}{5}\frac{G^3\eta}{c^5 b}\left(\frac{M}{b}\right)^3, \tag{28}$$

where $\eta \equiv \mu/M$ is the symmetric mass ratio. The minus sign here indicates the well-known result that gravitational waves induce an inspiral decay of the orbit until merger. The vector field perturbation considered here induces a similar inspiral effect, therefore enhancing the rate of inspiral and accelerating the merger (although $\dot{b}_A$ oscillates, and thus its sign can change with time). To leading order in vector field and gravitational wave perturbations, the total decay rate of the semimajor axis is simply the sum of Eqs. (27) and (28).

A comparison of the rate of change of the semimajor axis induced by the vector field and by gravitational waves is instructive. We can take the ratio of Eqs. (27) and (28) to find

$$\frac{(\dot{b}/b)_A}{(\dot{b}/b)_M} \sim \frac{c^3 b^4}{G^2\eta M^3\omega}\rho_A \sim 1.5\times 10^{-16}\frac{\eta^{-1}\rho_A}{0.3\,\frac{\mathrm{GeV}}{\mathrm{cm}^3}}\left(\frac{10^6 M_\odot}{M}\right)^{5/3}\left(\frac{10^{-5}\ \mathrm{Hz}}{f}\right)^{8/3}, \tag{29}$$

where we used the solar system dark-matter energy density as the reference value for ρ_A. From this ratio, we observe that the effects of the vector field are enhanced for asymmetric binaries that are widely separated, as we anticipated in Sec. I.

V. IMPACT ON GRAVITATIONAL WAVES

In this section we calculate the impact of the vector field dark-matter environment on the gravitational waves emitted by a quasicircular inspiraling compact binary. In Sec. V A, we review the calculation of the gravitational waveform in general relativity using the stationary-phase approximation. We also show how to perturb the gravitational waveform using the previous formalism. In Sec. V B, we calculate the dephasing of the gravitational wave due to the vector field dark-matter environment.

A. The stationary-phase approximation

We start by considering a linear perturbation of the metric around a Minkowski background as $g_{\mu\nu} = \eta_{\mu\nu} + h^M_{\mu\nu}$, with $|h^M_{\mu\nu}| \ll 1$. In general relativity, it is well known that gravitational waves in the far field can be expressed in a multipolar expansion. For a binary system and to leading order in post-Newtonian theory, one can write

$$h^{M,TT}_{ij} = \frac{2G}{c^4 D}\ddot{M}^{TT}_{ij}, \tag{30}$$

where D is the distance from the source to the detector in the source frame, the superscript TT indicates the transverse-traceless part of the tensor, and M_{ij} is the mass-quadrupole moment of the binary, with overhead dots standing for time derivatives. For a circular orbit of two point masses, the mass-quadrupole moment is given by

$$\ddot{M}_{11} = 2\mu(\pi f b)^2\cos(2\pi f t), \tag{31}$$

$$\ddot{M}_{22} = 2\mu(\pi f b)^2\sin(2\pi f t), \tag{32}$$

where f is the gravitational wave frequency, which is related to the orbital angular frequency via $\omega = \pi f$.

Gravitational waves in general relativity have only two polarizations, denoted h_+ and $h_\times$. One can thus write

$$h^{M,TT}_{ij} = h_+\begin{pmatrix}1&0&0\\0&-1&0\\0&0&0\end{pmatrix} + h_\times\begin{pmatrix}0&1&0\\1&0&0\\0&0&0\end{pmatrix}. \tag{33}$$

In this paper, we focus on the combination $h \equiv h_+ - ih_\times$. This combination can be parametrized as a product of a slowly varying amplitude $\mathcal{A}(t)$ and a rapidly oscillating phase $2\Phi(t)$ via

$$h(t) = \mathcal{A}(t)e^{2i\Phi(t)}. \tag{34}$$

Moreover, in this paper we will particularly focus on the Fourier transform of h, because most data analysis and parameter estimation for ground-based gravitational wave detectors is carried out in the frequency domain. In particular, we here use the convention

$$\tilde{h}(f) = \int \mathcal{A}(t)e^{i(2\Phi(t)-2\pi f t)}\,dt, \tag{35}$$

where the overhead tilde stands for the Fourier transform.

We can evaluate the Fourier transform with the stationary-phase approximation. In this approximation, we Taylor expand the exponent in the integrand of the Fourier transform around $t = t_*$, where t_* is a "stationary point" where $\dot{\Phi}(t_*) = \pi f$. Then, we have that

$$(2\Phi(t)-2\pi f t) \sim 2\Phi(t_*) - 2\pi f t_* + \ddot{\Phi}|_{t_*}(t-t_*)^2, \tag{36}$$

$$\mathcal{A}(t) \sim \mathcal{A}(t_*). \tag{37}$$

We can now solve the integral in Eq. (35) by integrating the remaining Gaussian to obtain

$$\tilde{h}(f) = i\tilde{\mathcal{A}}(t_*)\sqrt{\frac{\pi}{\ddot{\Phi}_*}}e^{i(2\Phi_* - 2\pi f t_*)} \equiv \tilde{\mathcal{A}}(f)e^{i\Psi(f)}. \tag{38}$$

Since $\tilde{\mathcal{A}}(f)$ is a slowly varying amplitude, $\tilde{h}(f)$ is controlled by the phase $\Psi(f)$. For gravitational wave interferometers, in fact, the Fourier phase is one of the most important elements of the waveform model. We can write the Fourier phase using that

$$\Phi(t_*) = \Phi_c - 2\pi \int_{f/2}^{\infty} \frac{F(F')}{\dot{F}(F')} dF', \tag{39}$$

$$t_* = t_c - \int_{f/2}^{\infty} \frac{1}{\dot{F}(F')} dF', \tag{40}$$

where F' is the integration variable, while $F = \omega/(2\pi)$ is the orbital frequency since $\dot{\Phi} = \omega$. The constants t_c and Φ_c are usually called the coalescence time and phase, respectively. Therefore, the Fourier phase can be written as

$$\Psi(f) = 2\Phi_c - 2\pi f t_c + 2\pi \int_{\frac{f}{2}}^{\infty} (f - 2F)\frac{dt}{dF} dF. \tag{41}$$

We can further massage Eq. (41) to put it into a form more amenable to computation. Let us begin by writing this equation in terms of the energy of the system,

$$\frac{dt}{dF} = \frac{dE}{dF}\mathcal{L}^{-1}, \tag{42}$$

where we used the balance law $\dot{E} \equiv -\mathcal{L}$ to relate the rate of change of the orbital energy of the binary $\dot{E}$ to the gravitational wave luminosity $\mathcal{L}$. With this in hand, the Fourier phase is given by

$$\Psi(f) = 2\pi f t_c - 2\Phi_c - 2\pi \int_{\infty}^{\frac{f}{2}} (2F - f)\mathcal{L}^{-1}\frac{dE}{dF} dF. \tag{43}$$

We thus have that, in the stationary-phase approximation, the phase of the gravitational wave is calculated as an integral of the binding energy E of the system and the luminosity $\mathcal{L}$ of the emitted gravitational wave. However, the binding energy and the luminosity may have other contributions apart from the ones from general relativity, such as modifications in E and $\mathcal{L}$ due to perturbations in the metric, the presence of a third body, modified theories of gravity, etc. Let us parametrize these contributions as

$$\mathcal{L} = \mathcal{L}_M + \delta\mathcal{L}, \tag{44}$$

$$E = E_M + \delta E, \tag{45}$$

where E_M and $\mathcal{L}_M$ are the binding energy of the orbit and luminosity of the gravitational wave, respectively, in general relativity and to as high a post-Newtonian order as one wishes to include. The quantities δE and $\delta\mathcal{L}$ represent corrections to E and $\mathcal{L}$ that are not from the binary. In this work, we focus on corrections that are only due to the presence of a vector field dark-matter environment. As we explained earlier, the vector field effect is conservative, because the perturbing force can be derived from the spatial gradient of a potential that is even under time reversal. In particular, the vector field environment that we consider does not induce radiative effects, since on the scales of interest to use, the vector field is not a propagating wave that carries energy momentum away from the binary. Therefore, the energy carried away in gravitational waves is the only source of energy loss. With this in mind, we conclude that $\delta\mathcal{L} = 0$ and $\delta E = V_A$, where V_A is given in Eq. (23).

The vector field generates a dephasing in the waveform through a perturbation in the binding energy of the orbit. To calculate such a modification, we start by writing the phase as

$$\Psi(f) = \Psi_M(f) + \Psi_A(f), \tag{46}$$

where $\Psi_M(f)$ is the Fourier gravitational wave phase to as high a post-Newtonian order as one wishes to include, while $\Psi_A(f)$ is the dephasing correction generated by the vector field environment. To find $\Psi_A(f)$, we insert the perturbed binding energy $\delta E = V_A$ of Eq. (23) into Eq. (43) to obtain

$$\Psi_A(f) = -2\pi \int^{\frac{f}{2}} (2F - f)\mathcal{L}_{\mathrm{M}}^{-1}\frac{dV_A}{dF} dF. \tag{47}$$

Observe that the evaluation of this integral requires that we convert between semimajor axis b and frequency F, which we can do through Kepler's third law to leading post-Newtonian order (i.e., $\omega^2 = M/b^3$), because the vector field perturbing force does not correct this expression.

There is another simple way to calculate the dephasing, which consists of calculating the perturbation in the orbital frequency of the binary as a function of time due to the presence of the vector field. That is, we split the variation of the frequency in a contribution from general relativity[6] plus the perturbation from the vector field, $\dot{F} = \dot{F}_M + \dot{F}_A$, with $\dot{F}_M \gg \dot{F}_A$. Then, we can calculate the dephasing as

[6]At leading order in post-Newtonian perturbation theory, the variation of the frequency in general relativity is given by $\dot{F}_M = \frac{3}{2}F(\dot{b}/b)_M$, with $(\dot{b}/b)_M$ given in Eq. (28).

$$\Psi_A(f) = -2\pi \int^{\frac{f}{2}} (2F - f) \frac{\dot{F}_A}{\dot{F}_M^2} dF. \tag{48}$$

We can now use Kepler law to relate the variation in the frequency with a variation in the semimajor axes, which we calculated in Eq. (25), as $\dot{F}_A = -\frac{3}{2} F (\dot{b}/b)_A$. In this way, we obtain an equivalent expression to the one given in Eq. (47).

With this in hand, the Fourier transform of the gravitational waves emitted by a quasicircular inspiraling compact binary in a vector dark-matter field environment can be written as

$$\tilde{h}(f) = \tilde{h}_M(f) e^{i\Psi_A(f)} \tag{49}$$

in the inspiral phase, where $\tilde{h}_M(f)$ is the Fourier transform of the gravitational wave combination h for a compact binary in isolation, in vacuum, and in general relativity. One can in fact use the highest post-Newtonian order expression for the Fourier phase $\Psi_M(f)$ in $\tilde{h}_M(f)$ when evaluating $\tilde{h}(f)$ if one wishes.

B. Calculation of the dephasing $\Psi_A(f)$

In order to solve the integral of Eq. (47), we need to calculate the variation of the binding energy with respect to the frequency. To do so, we follow the method of osculating orbits, and assume that the binding energy, to leading order, is given by the Newtonian expression, $E_M = -G\mu M/2b$. Then, the variations in the binding energy of the system are given by variations in the semimajor axes. Using the chain rule, we have that

$$\frac{dE_A}{dF} = \left(\frac{dE_A}{dt}\right)\left(\frac{dt}{dF}\right) = -E_M \left(\frac{dt}{dF}\right)_M \left(\frac{\dot{b}}{b}\right)_A, \tag{50}$$

where $(\dot{b}/b)_A$ is given by Eq. (27), while

$$\left(\frac{dt}{dF}\right)_M = -\frac{dE_M}{dF}\frac{1}{\mathcal{L}_M} = -\frac{5\pi}{48}\eta^{-1} M^2 (2\pi M F)^{-\frac{11}{3}}. \tag{51}$$

Inserting the above expressions in the integral of Eq. (47), and changing variables to $x = (2\pi F \mathcal{M})^{\frac{1}{3}}$ (with $\mathcal{M} = \eta^{3/5} M$ being the chirp mass), we have

$$\Psi_A(f) = \frac{25\pi G}{64} \sin(\alpha)^2 \mathcal{M}^2 \rho_A \int_\infty^{x(f/2)} dx (\pi f \mathcal{M} - x^3) \times \frac{1}{x^{20}} \cos\left(\frac{5\mathcal{M} m_A}{128 x^8} + \gamma\right) \sin\left(\frac{5}{128 x^5} - 2\varphi\right), \tag{52}$$

where we typically have $0.01 < x < 0.3$ for systems in the LISA band.

The above integral is highly oscillatory for the systems considered in this work, and thus, its solution is nontrivial. The oscillations have two characteristic timescales: one that is controlled by the chirp mass, and another that is dominated by the vector field mass. We thus solve the integral using the stationary-phase approximation again. We start by writing the integral as

$$\Psi_A(f) = \int_\infty^{x(f/2)} dx\, \mathcal{A}(x) e^{i\phi(x)}, \tag{53}$$

where $\mathcal{A}(x)$ is a slowly varying amplitude and

$$\phi(x) = \frac{5}{128 x^8}(x^3 - \mathcal{M} m_A) - 2\gamma. \tag{54}$$

We look for stationary points where $\phi'(x_{\rm stp}) = 0$, which yields $\pi f_{\rm stp} = 8 m_A/5$. Observe that the stationary point depends on the vector field mass m_A, but it is independent of the total mass of the binary M. Since we are integrating from $F = +\infty$, the integral is approximately zero until the stationary point $F \sim f_{\rm stp}$ is reached, so $\Psi_A(f) = 0$ for $F \gg f_{\rm stp}$. Once the stationary point is crossed, the integral has a contribution from the neighborhood of $f_{\rm stp}$ given by

$$\Psi_A(f) = \sqrt{\frac{5}{6}} \frac{15625\pi^{5/2} G \rho_A}{524288 \mathcal{M}^{5/2} m_A^{11/2}} (f_{\rm stp} - f) \times \sin(\alpha)^2 \sin\left(\xi - \frac{\pi}{4} + 2\varphi\right), \tag{55}$$

where we have defined $\xi = (75/32768) 5^{2/3} \times (\mathcal{M} m_A)^{-5/3} - \gamma$. For $F \ll f_{\rm stp}$, the integrand averages to zero again so the only contribution to the dephasing comes from the neighborhood of $F \sim f_{\rm stp}$, given by Eq. (55). Figure 3 shows the dephasing for an equal-mass binary with total mass $10^5 M_\odot$, and a vector field of mass $m_A = 10^{-18}$ eV. We calculate the dephasing under the stationary-phase approximation, and we also do so numerically, by explicitly integrating Eq. (52). Observe that our stationary-phase approximation to the solution of the integral accurately matches the numerical solution. The percentage error between the stationary-phase approximation and the numeric approach is $\ll 1\%$.

In the life cycle of binaries, the orbital (and gravitational wave) frequency chirps from small values, associated with the inspiral, to large values associated with the merger. The initial minimum value $f_{\rm min}$ is that at which we begin to observe the gravitational wave signal—we here take $f_{\rm min}$ to be either the lowest observable frequency in the LISA band, roughly 10^{-5} Hz, or the frequency four years before reaching merger. The maximum value $f_{\rm max}$ is that associated with the merger, which we can think of as roughly the innermost stable circular orbit (ISCO) frequency, $f_{\rm ISCO}$, for a test particle in a Schwarzschild black hole. Then, the solution given in Eq. (55) is valid for vector field

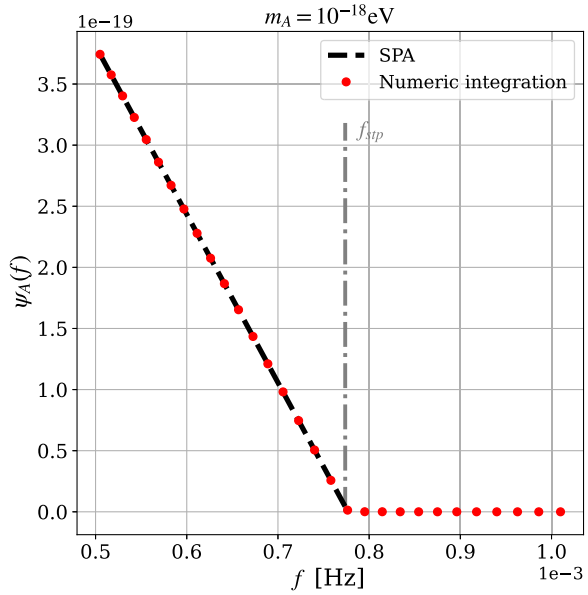

FIG. 3. Dephasing of the gravitational wave calculated as in Eq. (52) under the stationary-phase approximation (black dashed line) and numerically integrated (red dots), for $m = 10^{-18}$ eV, $M = 10^5 M_\odot$, $\eta = 0.25$, $\varphi = 0$, and $\alpha = \pi/4$. The vertical dash-dot gray line corresponds to the stationary point $\pi f_{\rm stp} = \frac{8}{5} m_A$. For $f > f_{\rm stp}$ the integral averages to zero. Observe that the stationary-phase approximation is very accurate, with percentage errors $\ll 1\%$ in the range shown.

dark-matter masses that are contained in the LISA band, namely, 10^{-19} eV $\lesssim m_A \lesssim 10^{-15}$ eV, and for systems where $f_{\rm ISCO} > f_{\rm stp}$. For systems such that $f_{\rm stp} < f_{\rm min}$ or $f_{\rm ISCO} < f_{\rm stp}$, the effect of the vector field dark-matter on the gravitational wave averages to zero.

VI. FISHER ANALYSIS

In this section, we present a Fisher analysis to compute the parameter space for which the dark-matter effect calculated in this manuscript can be detected in a gravitational wave observation. We start by defining the inner product between two waveforms h and g via

$$\langle h|g\rangle = 2\int_{f_{\rm min}}^{f_{\rm max}} \frac{\tilde{h}^*\tilde{g} + \tilde{h}\tilde{g}^*}{S_n} df, \tag{56}$$

where $S_n(f)$ is the *power noise spectrum* of the instrument, the overhead tilde stands for the Fourier transform, and the superscript star for complex conjugation. In this work, we focus on binary systems that can be detected in the LISA band, so we perform our analyses using an approximation to the LISA power noise spectrum [40].

With the inner product in hand, one can now define the *signal-to-noise ratio* for a given signal h as

$$\rho[h] = \langle h|h\rangle^{1/2}. \tag{57}$$

In general, the signal h depends on a set of parameters $\{\theta_i\}$ which are estimated by *matched filtering*. In the limit of $\rho[h] \gg 1$, and for Gaussian and stationary noise, one can show that the 1σ uncertainty in the estimation of parameters is given by

$$\Delta\theta^a \equiv \sqrt{\langle(\theta^a - \langle\theta^a\rangle)^2\rangle} = \sqrt{\Sigma^{aa}}, \tag{58}$$

where Σ^{aa} is the (a,a) diagonal element of the inverse of the covariance matrix (and summation is not implied here). The covariance matrix, also known as the *Fisher information matrix* Γ_{ab}, is defined as

$$\Gamma_{ab} = \left\langle \frac{\partial h}{\partial\theta_a} \middle| \frac{\partial h}{\partial\theta_b} \right\rangle. \tag{59}$$

We wish to perform a Fisher analysis to estimate the accuracy to which we could measure dark-matter parameters contained in the dephasing of Eq. (55) with a future LISA gravitational wave observation. To do so, it is convenient to parametrize the dephasing of the gravitational wave in terms of two parameters, as

$$\Psi_A(f) = \beta\left(1 - \frac{f}{f_{\rm stp}}\right)\theta(f_{\rm stp} - f), \tag{60}$$

where $\pi f_{\rm stp} = \frac{8}{5} m_A$ and β is given by

$$\begin{aligned}\beta &\sim \sqrt{\frac{5}{6}} \frac{625\pi^{3/2} G\rho_A}{65536 \mathcal{M}^{5/2} m_A^{9/2}} \sin(\alpha)^2 \\ &\sim 3\times 10^{-12} \frac{\rho_A}{0.3\,\frac{\rm GeV}{\rm cm^3}} \left(\frac{10^4 M_\odot}{M}\right)^{5/2} \left(\frac{10^{-19}\ {\rm eV}}{m_A}\right)^{9/2}.\end{aligned} \tag{61}$$

We then add these two parameters to the rest of the parameters contained in the vacuum part of the gravitational wave signal $\tilde{h}_M$ in Eq. (49), which in this paper we will model through a TaylorF2 model [41], valid only up to the ISCO, namely,

$$\begin{aligned}\Psi_M = 2\pi f t_c - \Phi_c - \frac{\pi}{4} + \frac{3}{128} U^{-5/3} - \frac{3\pi}{8}\eta^{-3/5} U^{-2/3} \\ + \frac{5}{96}\eta^{-2/5}\left(\frac{743}{336} + \frac{11\eta}{4}\right) U^{-1},\end{aligned} \tag{62}$$

with $U = \pi\mathcal{M}f$. Equation (49) then gives us our dark-matter enhanced waveform model.

The Fisher estimate of the accuracy to which dark-matter parameters can be measured with a future gravitational wave observation can be carried out in various ways. In this paper, we consider the hypothetical scenario that the true gravitational wave signal did *not* contain any dark-matter effects (e.g., because there was no dark-matter near this particular binary), and then we ask how well we can ascertain that the dark-matter density ρ_A (or the dephasing parameter β) is consistent with zero. In a Bayesian language, we expect that a Bayesian parameter estimation

study of such a hypothetical signal with our model would yield approximately Gaussian marginalized posteriors centered at $\beta = 0$, and we wish to determine the width of this distribution. The 1σ width is then given by Eq. (58), with the Fisher matrix evaluated for the $a = \beta$ parameter, and setting $\beta = 0$ after taking the β derivatives.

From these considerations, it is clear that we first need to calculate the following derivatives (besides the derivatives with respect to the usual vacuum parameters that characterize $\tilde{h}_M$) to compute the Fisher matrix:

$$\frac{\partial \tilde{h}(f)}{\partial \beta} = i\left(1 - \frac{f}{f_{\rm stp}}\right)\theta(f - f_{\rm stp})\tilde{h}(f), \tag{63}$$

$$\frac{\partial \tilde{h}(f)}{\partial f_{\rm stp}} = i\beta\left[\frac{f}{f_{\rm stp}^2}\theta(f - f_{\rm stp}) + \left(1 - \frac{f}{f_{\rm stp}}\right)\delta(f - f_{\rm stp})\right]\tilde{h}(f). \tag{64}$$

Observe that the derivative with respect to $f_{\rm stp}$ does not contribute to the Fisher matrix because we perform the analysis for the fiducial value $\beta = 0$, so every matrix element containing such derivative vanishes. Therefore, we drop $f_{\rm stp}$ from the parameters list to perform the Fisher analysis.

For systems with $f_{\rm stp} < f_{\rm min}$, the effect of the vector field dark-matter on the orbit averages to zero—this is the region where the step function always vanishes. On the other hand, for binaries with $f_{\rm ISCO} < f_{\rm stp}$, the dephasing is degenerate with ϕ_c and t_c, and thus β also cannot be measured. However, for systems whose frequency chirps *through* the stationary frequency $f_{\rm stp}$ in the period of observation, the degeneracy is broken as a consequence of the step function turning on during the observation time. We thus consider systems for which, in the period of observation, the frequency takes the value $f_{\rm stp}$ at some point in the chirp of the binary.

Figure 4 shows the gravitational wave characteristic strain for different binary masses as a function of the gravitational wave frequency. The black solid curve is the characteristic LISA sensitivity strain [40]. For each binary mass, we show the frequency range each binary sweeps through. The initial frequency $f_{\rm min}$ is calculated as the frequency the binary had four years before ISCO, corresponding to a large observation period with LISA. Observe that each frequency range also corresponds to the mass range of the vector field that could be tested with a gravitational wave observation. This is because, as mentioned before, for each binary evolution, the orbital frequency resonates with the vector field mass at some point in the evolution of the binary, activating the step function and thus breaking the degeneracy. In particular, we see that for systems that could be probed by LISA, the mass range for the vector field that could be tested in a detection is $m_A \sim (10^{-19}, 10^{-15})$ eV.

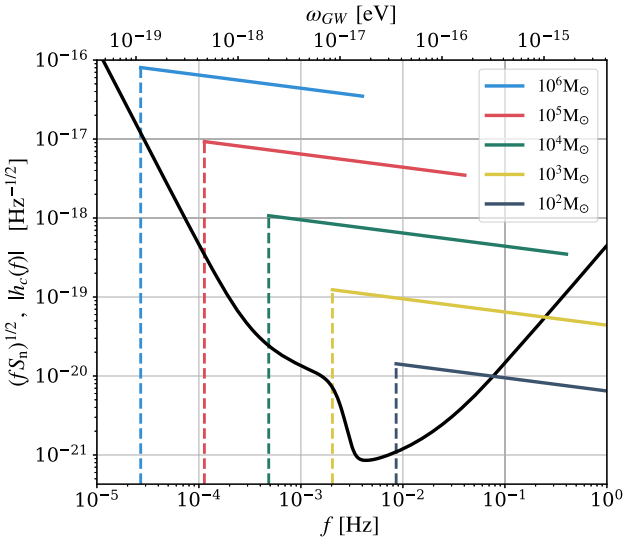

FIG. 4. LISA's sensitivity strain (black curve). The different colors indicate the gravitational wave characteristic strain for each binary mass during the inspiral, defined as $|h_c(f)| = 2f|\mathcal{A}(f)|$. We consider symmetric-mass binaries at $D_L = 1$ Gpc. The mass of each member of the binary is the one indicated in the label. The dashed lines indicate $f_{\rm min}$ for each system, calculated as the frequency four years before the ISCO is reached (corresponding to LISA's observation period). On the top axes we show $\omega_{\rm GW} \equiv 2\pi f$.

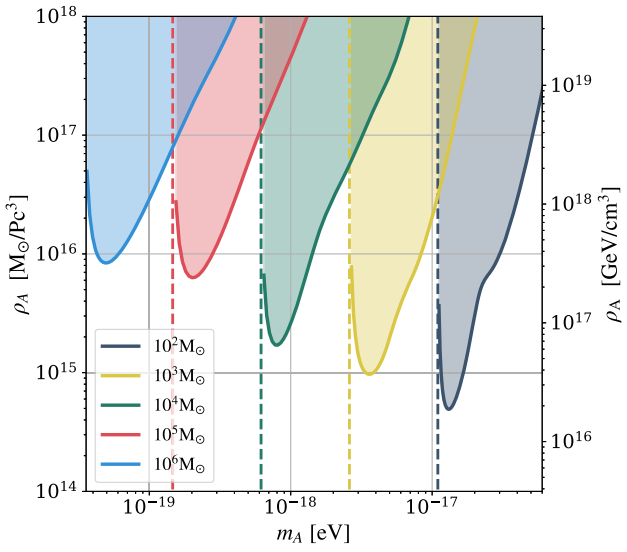

FIG. 5. 1σ accuracy (estimated with a Fisher analysis) to which ρ_A can be measured, given a value of the vector mass in eV, for a binary with various total masses (shown with different colors). The vertical dash-dot lines indicate $f_{\rm min}$, corresponding to the frequency of the system four years before the ISCO. We assume $\eta = 0.25$ for the analysis. If a binary system is immersed in a dark-matter vector environment with a density larger than these values (shaded regions), then the gravitational waves emitted carry a dark-matter signature that is detectable with LISA for a four-year observation.

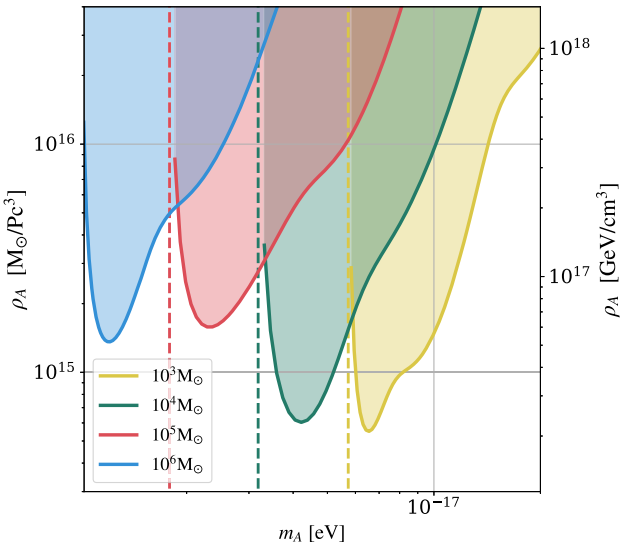

FIG. 6. 1σ accuracy (estimated with a Fisher analysis) to which ρ_A can be measured, given a value of the vector mass in eV, for a binary with various total masses (shown with different colors). The vertical dash-dot lines indicate $f_{\rm min}$, corresponding to the frequency of the system four years before the ISCO. For this analysis, we assume binary systems with asymmetric masses, where the heavier mass is given for each color, and the lightest mass is always $10^2 M_\odot$. If a binary system is immersed in a dark-matter vector environment with a density larger than these values (shaded regions), then the gravitational waves emitted carry a dark-matter signature that is detectable with LISA for a four-year observation. We can see that the effect is greater than in the symmetric case (Fig. 5).

Figure 5 shows the 1σ accuracy (estimated with a Fisher analysis) to which ρ_A can be measured, as a function of the vector field mass for five different future LISA observations of equal-mass binaries with different total masses. The shaded regions corresponds to values of the dark-matter density for which the vector field dark-matter effects we considered in this paper would leave a measurable (with LISA) impact on the gravitational waves emitted. Although the fiducial value for the dark-matter density in our Solar System is $\rho_{\rm DM} \sim 0.3$ GeV/cm^3, this density could be significantly larger near supermassive black holes. We thus see that LISA opens the window to probing a new regime of vector dark-matter densities with gravitational waves. In Fig. 6 we show the same analysis as for Fig. 5, but considering asymmetric systems. In particular, we consider systems where the lighter black hole in the binary has a mass of $10^2 M_\odot$, while the heavier companion's mass is given by the label of each curve. We can see that, for asymmetric masses, the dark-matter effect is enhanced with respect to symmetric binaries, as was expected from Eq. (29).

VII. CONCLUSIONS

In this work, we studied the dephasing in the gravitational waves emitted by compact binaries due to an ultralight vector dark-matter field environment. Ultralight fields produce oscillating gravitational potentials that are approximately homogeneous at the characteristic scales of compact binary systems. These oscillations perturb the orbit, producing a variation in the binding energy of the system. We showed that such perturbations generated a dephasing in the gravitational waves emitted by the binary and calculated explicitly the Fourier phase of the signal. We found that the dark-matter correction to the Fourier phase was proportional to the dark-matter energy density in the local patch, ρ_A. We also showed that the dark-matter effect can be important when the frequency of the gravitational wave resonates with the vector field mass at some point in the evolution of the binary.

We performed a Fisher analysis to estimate the accuracy to which we may be able to constrain the dark-matter density ρ_A with a future LISA observation. We found that four-year LISA observations should allow us to measure dark-matter densities larger than 10^{16} GeV/cm^3 for vector masses in the range $(10^{-19}, 10^{-16})$ eV. We also found that these measurements were best for asymmetric binaries with low total mass. Interestingly, some of these are systems whose merger could potentially also be observed by LIGO, after LISA observes the early inspiral [42]. Such multi-wavelength gravitational wave events seem ideal to probe nonvacuum or beyond-Einstein effects in gravitational wave signals [43,44]. Therefore, future LISA observations of the gravitational waves emitted in the quasicircular inspiral of massive black holes may detect or yield interesting constraints on the density of vector-type ultralight dark-matter surrounding binary black hole systems.

Future work could focus on a complete study of the perturbations in the gravitational waveform due to the presence of a vector field environment. Such a study should include perturbations in the waveform resulting from the variation of other orbital parameters, in addition to the variation of the semimajor axes considered here. In particular, future work could focus on the variation of the inclination of the orbital plane, which has an impact on the amplitude of the gravitational wave. Also, the formalism presented in this manuscript can be generalized for eccentric orbits [45], since the vector field also has an impact on the evolution of the eccentricity of the orbits.

ACKNOWLEDGMENTS

We thank Esteban Calzetta for useful discussions. N. Y. acknowledges support from the Simons Foundation through Award No. 896696, the NSF through Grant No. PHY-2207650, and NASA through Grant No. 80NSSC22K0806. T. F. C. and D. L. N. acknowledge support from CONICET and UBA.

DATA AVAILABILITY

No data were created or analyzed in this study.

APPENDIX: BINARY SYSTEMS IN ULTRALIGHT DARK-MATTER HALOS

In this appendix, we discuss the validity of approximating the dark-matter energy profile as homogeneous on the extension of the orbit. Numerical solutions show that dark-matter halos in ultralight dark-matter models can be described by solitonic cores surrounded by Navarro-Frenk-White profiles. The radial density profile of the core can be modeled as [23,46,47]

$$\rho_c \sim \rho_{c,0}[1 + 0.091(r/r_c)]^{-8}, \tag{A1}$$

with

$$\rho_{c,0} \sim 1.9 \times 10^{-10} \left(\frac{10^{-18}\ \text{eV}}{m_A}\right)^2 \left(\frac{\text{kpc}}{r_c}\right)^4 \frac{M_\odot}{\text{pc}^3}, \tag{A2}$$

where r_c is the core radius, defined as the radius at which the density drops to half of its peak value. The mass of the core is defined as the mass enclosed by r_c. For ultralight scalar field models, the core radius can be related to the dark-matter field mass and the corresponding total halo masses. At redshift $z = 0$, r_c can be estimated as[7]

$$r_c = 10^{11} \left(\frac{10^{-18}\ \text{eV}}{m_A}\right) \left(\frac{M_{\text{halo}}}{10^{12} M_\odot}\right)^{-1/3} \text{km}. \tag{A3}$$

If we suppose that each halo hosts a galaxy with a supermassive black hole at its center [48,49], we can further relate the mass of the black hole with the mass of the dark-matter halo as [50–52]

$$M \sim 10^7 M_\odot \left(\frac{M_{\text{halo}}}{10^{12} M_\odot}\right)^\kappa, \tag{A4}$$

where $\kappa \sim 1.6$.

In order to explain our setup, we consider the case of supermassive and low/intermediate massive binaries separately. In the case of supermassive black hole binaries, it is reasonable to assume that, due to processes such as dynamical friction and mass segregation, the black holes are most probably located near the center of their host galaxy. Moreover, these galaxies themselves are typically located near the core centers of their respective halos [53,54], where the energy density is approximately constant [see Eq. (A1)]. Then, if the size of the orbit b is much smaller than the size of the core r_c, we can assume that the energy profile throughout the binary is approximately homogeneous. To check the validity of this assumption, we consider a supermassive binary of $M = 10^6 M_\odot$, which corresponds to the largest system LISA can probe. Using Eq. (A4) for this system, we obtain a halo mass of approximately $M_{\text{halo}} = 10^{11} M_\odot$, and from Eq. (A3), for a field environment of mass $m_A = 10^{-18}$ eV, we obtain a corresponding central core of radius $r_c = 2.5 \times 10^{11}$ km. We thus see that the core size is much larger than the orbits considered in this work [see Eq. (6)], so we can assume an approximately homogeneous energy density profile in the extension of the orbit. Also, we see that this estimate matches the one from the discussion in Sec. II regarding the de Broglie wavelength given in Eq. (5), since we used the velocity dispersion of the Milky Way, which hosts a supermassive black hole at its center (Sag. A*) of $\sim 4 \times 10^6 M_\odot$, and has a halo mass of $\sim 7 \times 10^{11} M_\odot$.

For supermassive binaries, there is also non-negligible backreaction of the binary on the dark-matter field environment. Numerical simulations of inspiraling supermassive binaries in ultralight dark-matter field environments show that this backreaction generates a quasistationary energy density profile around the binary, which is approximately homogeneous throughout the extension of the orbit, and is peaked in the vicinity of the black holes (see, for instance, Refs. [55–57]). This energy profile can be understood as a local enhancement of the host soliton density profile, produced by the accretion of dark-matter by the black holes. The effect is maximal when the orbital radius r_{12} is of order of the Compton wavelength λ_c of the field. In our case, the orbital radius of the systems satisfies $r_{12} \ll \lambda_c$. We here ignore this effect, so the values used for the density of the dark-matter field in the orbit are in general underestimated. A larger density would only enhance the effects considered here, making our estimates necessarily conservative.

Finally, we consider the case of intermediate- and low-mass black hole binaries. These systems are much smaller in spatial extent than the supermassive ones, since the radius of the orbit scales as the total mass of the binary. Even if they are not at the center of the core, it is most probable that the orbit is still completely embedded in it, or in an interference granule of characteristic size given by λ_{dB}. This means that they can be considered to be inside a region where the vector field is assumed to be homogeneous. Furthermore, because of its low mass, the backreaction of the binary over the halo can be neglected. Then, we can assume that the vector field is homogeneous through the orbit of intermediate- and low-mass binaries, as done throughout this work.

[7] See, for instance, Eq. (7) in Ref. [46].

[1] E. G. M. Ferreira, Ultra-light dark matter, Astron. Astrophys. Rev. **29**, 7 (2021).
[2] R. Hlozek, D. Grin, D. J. E. Marsh, and P. G. Ferreira, A search for ultralight axions using precision cosmological data, Phys. Rev. D **91**, 103512 (2015).
[3] T. F. Chase and D. López Nacir, Ultralight vector dark matter, anisotropies, and cosmological adiabatic modes, Phys. Rev. D **109**, 083521 (2024).
[4] T. F. Chase, M. Leizerovich, D. López Nacir, and S. Landau, Cosmological perturbations with ultralight vector dark matter fields: Numerical implementation in class, Phys. Rev. D **111**, 103520 (2025).
[5] D. Blas, D. López Nacir, and S. Sibiryakov, Secular effects of ultralight dark matter on binary pulsars, Phys. Rev. D **101**, 063016 (2020).
[6] D. Blas, D. L. Nacir, and S. Sibiryakov, Ultralight dark matter resonates with binary pulsars, Phys. Rev. Lett. **118**, 261102 (2017).
[7] D. López Nacir and F. R. Urban, Vector fuzzy dark matter, fifth forces, and binary pulsars, J. Cosmol. Astropart. Phys. 10 (2018) 044.
[8] L. Blanchet, Post-Newtonian theory for gravitational waves, Living Rev. Relativity **17**, 2 (2014).
[9] N. Yunes, B. Kocsis, A. Loeb, and Z. Haiman, Imprint of accretion disk-induced migration on gravitational waves from extreme mass ratio inspirals, Phys. Rev. Lett. **107**, 171103 (2011).
[10] B. Kocsis, N. Yunes, and A. Loeb, Observable signatures of EMRI black hole binaries embedded in thin accretion disks, Phys. Rev. D **84**, 024032 (2011).
[11] L. Speri, A. Antonelli, L. Sberna, S. Babak, E. Barausse, J. R. Gair, and M. L. Katz, Probing accretion physics with gravitational waves, Phys. Rev. X **13**, 021035 (2023).
[12] P. S. Cole, G. Bertone, A. Coogan, D. Gaggero, T. Karydas, B. J. Kavanagh, T. F. M. Spieksma, and G. M. Tomaselli, Distinguishing environmental effects on binary black hole gravitational waveforms, Nat. Astron. **7**, 943 (2023).
[13] E. Barausse, V. Cardoso, and P. Pani, Can environmental effects spoil precision gravitational-wave astrophysics?, Phys. Rev. D **89**, 104059 (2014).
[14] D. Baumann, H. S. Chia, and R. A. Porto, Probing ultralight bosons with binary black holes, Phys. Rev. D **99**, 044001 (2019).
[15] M. Bošković, M. Koschnitzke, and R. A. Porto, Signatures of ultralight bosons in the orbital eccentricity of binary black holes, Phys. Rev. Lett. **133**, 121401 (2024).
[16] M. Baryakhtar, R. Lasenby, and M. Teo, Black hole superradiance signatures of ultralight vectors, Phys. Rev. D **96**, 035019 (2017).
[17] P. Pani, V. Cardoso, L. Gualtieri, E. Berti, and A. Ishibashi, Black hole bombs and photon mass bounds, Phys. Rev. Lett. **109**, 131102 (2012).
[18] M. J. Stott, Ultralight Bosonic Field Mass Bounds from Astrophysical Black Hole Spin, p. 9, 2020.
[19] P. Brax, P. Valageas, C. Burrage, and J. A. R. Cembranos, Detecting dark matter oscillations with gravitational waveforms, Phys. Rev. D **110**, 083515 (2024).
[20] A. Marriott-Best, M. Peloso, and G. Tasinato, New gravitational wave probe of vector dark matter, Phys. Rev. D **111**, 103511 (2025).
[21] M. A. Amin, M. Jain, R. Karur, and P. Mocz, Small-scale structure in vector dark matter, J. Cosmol. Astropart. Phys. 08 (2022) 014.
[22] G. P. Centers *et al.*, Stochastic fluctuations of bosonic dark matter, Nat. Commun. **12**, 7321 (2021).
[23] H.-Y. Schive, T. Chiueh, and T. Broadhurst, Cosmic structure as the quantum interference of a coherent dark wave, Nat. Phys. **10**, 496 (2014).
[24] J. N. López-Sánchez, E. Munive-Villa, C. Skordis, and F. R. Urban, Scaling relations and tidal disruption in spin *s* ultralight dark matter models, p. 2 2025.
[25] J. Bovy and S. Tremaine, On the local dark matter density, Astrophys. J. **756**, 89 (2012).
[26] J. N. Bahcall, K giants and the total amount of matter near the sun, Astrophys. J. **287**, 926 (1984).
[27] M. Alcubierre, J. Barranco, A. Bernal, J. C. Degollado, A. Diez-Tejedor, M. Megevand, D. Nú nez, and O. Sarbach, Gravitational atoms beyond the test field limit: The case of Sgr A* and ultralight dark matter, Classical Quantum Gravity **42**, 21LT01 (2025).
[28] E. Y. Davies and P. Mocz, Fuzzy dark matter soliton cores around supermassive black holes, Mon. Not. R. Astron. Soc. **492**, 5721 (2020).
[29] A. Cruz-Osorio, F. S. Guzmán, and F. D. Lora-Clavijo, Scalar field dark matter: Behavior around black holes, J. Cosmol. Astropart. Phys. 06 (2011) 029.
[30] N. Bar, K. Blum, T. Lacroix, and P. Panci, Looking for ultralight dark matter near supermassive black holes, J. Cosmol. Astropart. Phys. 07 (2019) 045.
[31] M. Aghaie, G. Armando, A. Dondarini, and P. Panci, Bounds on ultralight dark matter from NANOGrav, Phys. Rev. D **109**, 103030 (2024).
[32] F. Hancock and H. Witek, Black-hole hair from vector dark matter accretion, Phys. Rev. D **112**, 044033 (2025).
[33] D. W. P. Amaral, M. Jain, M. A. Amin, and C. Tunnell, Vector wave dark matter and terrestrial quantum sensors, J. Cosmol. Astropart. Phys. 06 (2024) 050.
[34] J. Veltmaat, J. C. Niemeyer, and B. Schwabe, Formation and structure of ultralight bosonic dark matter halos, Phys. Rev. D **98**, 043509 (2018).
[35] I.-K. Liu, N. P. Proukakis, and G. Rigopoulos, Coherent and incoherent structures in fuzzy dark matter haloes, Mon. Not. R. Astron. Soc. **521**, 3625 (2023).
[36] L. Bieri, D. Garfinkle, and N. Yunes, Gravitational wave memory in ΛCDM cosmology, Classical Quantum Gravity **34**, 215002 (2017).
[37] C. W. Misner, K. S. Thorne, and J. A. Wheeler, *Gravitation* (W. H. Freeman, San Francisco, 1973).
[38] E. Poisson and C. M. Will, *Gravity: Newtonian, Post-Newtonian, and General Relativistic* (Cambridge University Press, Cambridge, England, 2016).
[39] P. C. Peters, Gravitational radiation and the motion of two point masses, Phys. Rev. **136**, B1224 (1964).
[40] T. Robson, N. J. Cornish, and C. Liu, The construction and use of LISA sensitivity curves, Classical Quantum Gravity **36**, 105011 (2019).
[41] T. Damour, B. R. Iyer, and B. S. Sathyaprakash, A comparison of search templates for gravitational waves from binary inspiral, Phys. Rev. D **63**, 044023 (2001); **72**, 029902 (E) (2005).

[42] A. Sesana, Prospects for multiband gravitational-wave astronomy after GW150914, Phys. Rev. Lett. **116**, 231102 (2016).
[43] E. Barausse, N. Yunes, and K. Chamberlain, Theory-agnostic constraints on black-hole dipole radiation with multiband gravitational-wave astrophysics, Phys. Rev. Lett. **116**, 241104 (2016).
[44] S. E. Perkins, N. Yunes, and E. Berti, Probing fundamental physics with gravitational waves: The next generation, Phys. Rev. D **103**, 044024 (2021).
[45] N. Yunes, K. G. Arun, E. Berti, and C. M. Will, Post-circular expansion of eccentric binary inspirals: Fourier-domain waveforms in the stationary phase approximation, Phys. Rev. D **80**, 084001 (2009); **89**, 109901(E) (2014).
[46] H.-Y. Schive, M.-H. Liao, T.-P. Woo, S.-K. Wong, T. Chiueh, T. Broadhurst, and W. Y. P. Hwang, Understanding the core-halo relation of quantum wave dark matter from 3D simulations, Phys. Rev. Lett. **113**, 261302 (2014).
[47] B. Schwabe, J. C. Niemeyer, and J. F. Engels, Simulations of solitonic core mergers in ultralight axion dark matter cosmologies, Phys. Rev. D **94**, 043513 (2016).
[48] J. Kormendy and D. Richstone, Inward bound: The search for supermassive black holes in galactic nuclei, Annu. Rev. Astron. Astrophys. **33**, 581 (1995).
[49] L. Ferrarese and D. Merritt, A fundamental relation between supermassive black holes and their host galaxies, Astrophys. J. Lett. **539**, L9 (2000).
[50] L. Ferrarese, Beyond the bulge: A fundamental relation between supermassive black holes and dark matter halos, Astrophys. J. **578**, 90 (2002).
[51] C. M. Booth and J. Schaye, Dark matter haloes determine the masses of supermassive black holes, Mon. Not. R. Astron. Soc. **405**, L1 (2010).
[52] K. Bandara, D. Crampton, and L. Simard, A relationship between supermassive black hole mass and the total gravitational mass of the host galaxy, Astrophys. J. **704**, 1135 (2009).
[53] A. V. Kravtsov, A. A. Berlind, R. H. Wechsler, A. A. Klypin, S. Gottloeber, B. Allgood, and J. R. Primack, The Dark side of the halo occupation distribution, Astrophys. J. **609**, 35 (2004).
[54] A. A. Berlind, D. H. Weinberg, A. J. Benson, C. M. Baugh, S. Cole, R. Dave, C. S. Frenk, A. Jenkins, N. Katz, and C. G. Lacey, The halo occupation distribution and the physics of galaxy formation, Astrophys. J. **593**, 1 (2003).
[55] J. Bamber, J. C. Aurrekoetxea, K. Clough, and P. G. Ferreira, Black hole merger simulations in wave dark matter environments, Phys. Rev. D **107**, 024035 (2023).
[56] J. C. Aurrekoetxea, K. Clough, J. Bamber, and P. G. Ferreira, Effect of wave dark matter on equal mass black hole mergers, Phys. Rev. Lett. **132**, 211401 (2024).
[57] R. Boey, E. Kendall, Y. Wang, and R. Easther, Supermassive binaries in ultralight dark matter solitons, Phys. Rev. D **112**, 023510 (2023).